Probing the superconducting ground state of ZrIrSi: A muon spin rotation and relaxation study

K. Panda,[1] A. Bhattacharyya,[1,*] D. T. Adroja,[2,3] N. Kase,[4] P. K. Biswas,[2] Surabhi Saha,[5] Tanmoy Das,[5,†] M. R. Lees,[6] and A. D. Hillier[2]

[1]*Department of Physics, Ramakrishna Mission Vivekananda Educational and Research Institute, Howrah 711202, India*
[2]*ISIS Facility, Rutherford Appleton Laboratory, Chilton, Didcot, Oxon OX11 0QX, United Kingdom*
[3]*Highly Correlated Matter Research Group, Physics Department, University of Johannesburg, Auckland Park 2006, South Africa*
[4]*Department of Applied Physics, Tokyo University of Science, Tokyo 125-8585, Japan*
[5]*Department of Physics, Indian Institute of Science, Bangalore 560012, India*
[6]*Department of Physics, University of Warwick, Coventry CV4 7AL, United Kingdom*

(Received 21 March 2019; revised manuscript received 24 April 2019; published 21 May 2019)

The superconducting ground state of recently discovered ZrIrSi is probed by means of muon spin rotation and relaxation (μSR) and resistivity measurements. The occurrence of superconductivity at $T_C = 1.7$ K is confirmed by resistivity measurements. Zero field μSR study revealed that below T_C there is no spontaneous magnetic field in the superconducting state, which indicates time-reversal symmetry is preserved in the case of ZrIrSi. From transverse field μSR measurement, we have estimated the superfluid density as a function of temperature, which is described by an isotropic *s*-wave model with a superconducting gap $2\Delta(0)/k_BT_C = 5.10(2)$ and indicates the presence of strong coupling superconductivity. *Ab initio* electronic structure calculation indicates that there are four bands passing through the Fermi level, forming four Fermi surface pockets. We find that the low-energy bands are dominated by the 4*d* orbitals of the transition metal Zr, with substantially less weight from the 5*d* orbitals of the Ir atoms.

DOI: 10.1103/PhysRevB.99.174513

I. INTRODUCTION

Recently, a number of studies have been carried out in ternary metal phosphide, silicide, and arsenide with the general formula $TrT'X$ (Tr and T' are either 4*d* or 3*d* transition elements, whereas X is either a group IV or a group V member) [1–10]. These systems have attracted considerable attention due to their relatively high superconducting transition temperature (T_C), for example, 15.5 K for hexagonal *h*-MoNiP [8], 13 K for *h*-ZrRuP [11], and 12 K for *h*-ZrRuAs [12]. These ternary equiatomic systems provide a structure in which to investigate the role of spin-orbit (SO) coupling in superconductivity, which has not been so well studied in these systems. Compounds with Ir are often characterized by a strong SO coupling effect, due to the presence of the Ir 5*d* orbitals. Superconductivity is observed in a number of Ir-based compounds such as Li_2IrSi_3 ($T_C = 4.2$ K) [13,14], IrGe ($T_C = 4.7$ K) [15], RIr_3 [$T_C = 3.1$ K (La), $T_C = 3.3$ K (Ce)] [16–18], $CaIr_2$($T_C = 5.8$ K) [19], HfIrSi ($T_C = 3.1$ K) [20], and ScIrP ($T_C = 3.4$ K) [21]. Cuamba *et al.* [13–15,22] suggest that the presence of strong SO coupling and a significant contribution to the total density of states (DOS) come from the Ir atom in most of the Ir-based compounds. Recently, we have reported time-reversal symmetry (TRS) breaking superconductivity on the transition-metal-based caged-type $R_5Rh_6Sn_{18}$ (R = Lu, Sc, and Y) [23–25] compounds due to strong spin-orbit coupling.

In ternary equiatomic compounds, superconductivity has only been found in two types of crystal structures: the first is the hexagonal Fe_2P type (space group $P\bar{6}m2$) [4,6,8], and the second is the orthorhombic Co_2Si type (space group *Pnma*) [2,4,7,8]. It is interesting to note that in these systems T_C is strongly associated with crystal structure. Furthermore, the *h*-Fe_2P-type structure exhibits a T_C higher than that of the *o*-Co_2Si-type structure, for example: *h*-ZrRuP has a T_C at 13.0 K, whereas *o*-ZrRuP has a T_C at 3.5 K. In the case of the *h*-Fe_2P-type structure each layer is filled with either Tr and T' or X and X elements. In the case of *o*-ZrRuP, Shirotani *et al.* [9] reported the formation of two-dimensional triangular Ru_3 clusters that are connected in the basal plane through Ru-P ionic bonds. They are also connected through Zr-Ru bonds where Zr atoms occupy the $z = 1/2$ plane. If phosphorus is replaced by the more electronegative silicon then the nearest-neighbor Ru-Ru bond length is enlarged to 2.87 Å. Surprisingly *o*-MoRuP shows superconductivity at 15.5 K, which is as high as isoelectronic *h*-ZrRuP ($T_C = 13$ K) and *h*-MoNiP ($T_C = 13$ K). Ching *et al.* [4] have shown that in *o*-MoRuP and *o*-ZrRuP a higher value of the DOS at the Fermi level is directly related to higher T_C, as suggested for a BCS superconductor. In these systems, the density of states are governed by Mo 4*d* orbitals. Ching *et al.* [4] have calculated the values of the density of states, which are 0.46 states per eV atom and 0.33 states per eV atom for *o*-MoRuP and *o*-ZrRuP, respectively.

Therefore, to investigate the superconducting pairing mechanism in ZrIrSi, we have conducted a systematic muon spin rotation and relaxation (μSR) study. Zero field (ZF) μSR is a powerful technique to determine whether TRS

*amitava.bhattacharyya@rkmvu.ac.in
†tnmydas@gmail.com

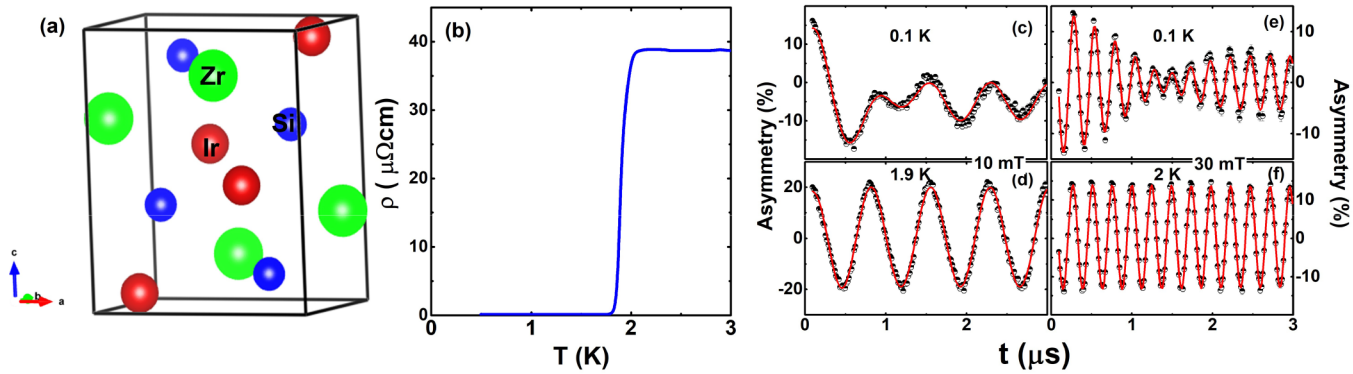

FIG. 1. (a) The crystal structure of ZrIrSi which crystallizes in the orthorhombic structure with the space group *Pnma*, where the spheres represent the Zr (green), Ir (red), and Si (blue) atoms. (b) Temperature variation of resistivity in zero field. Time dependence TF-μSR asymmetry spectra for ZrIrSi recorded at (c) $T = 0.1$ K and (d) $T = 1.9$ K in the presence of the applied field $\mu_0 H = 10$ mT and at (e) $T = 0.1$ K and (f) $T = 2.0$ K in the applied field $\mu_0 H = 30$ mT. The red solid line shows the fittings to the data using Eq. (1) described in the text.

breaking occurs in the superconducting state [26]. ZF-μSR for ZrIrSi data indicate the absence of any spontaneous magnetic fields below T_C, thus implying that TRS is not broken in the superconducting state. The superfluid density as a function of temperature is determined from the depolarization rate of the transverse field (TF) μSR which is well described by an isotropic *s*-wave model. These results are further supported by *ab initio* electronic structure calculation.

II. EXPERIMENTAL DETAILS

For this study, a polycrystalline sample of ZrIrSi was synthesized using a typical arc melting process on a water-cooled copper hearth using Zr (99.99%), Ir (99.99%), and Si (99.999%) in a stoichiometric ratio. The ingot was remelted several times to improve the phase homogeneity. The sample was then annealed at 1000 °C for a week in a sealed vacuum quartz tube. X-ray diffraction was carried out using Cu-K_α radiation. Electrical resistivity measurements were made using a standard dc four-probe technique down to 0.5 K.

μSR experiments were performed at the ISIS pulsed neutron and muon source of Rutherford Appleton Laboratory, UK, using a MuSR spectrometer with 64 detectors at transverse and longitudinal directions [27]. One hundred percent spin-polarized muons were implanted into the sample. The muons decay with an average lifetime of 2.2 μs producing two neutrinos and a positron, which is emitted in a direction that is related to orientation of the muon spin vector at the time of the decay. These positrons were detected by the detectors, placed in either the forward (F) or the backward (B) direction. The time dependence of the μSR asymmetry spectra A was calculated as $A(t) = \frac{N_F(t) - \alpha N_B(t)}{N_F(t) + \alpha N_B(t)}$, where $N_F(t)$ and $N_B(t)$ are the number of positrons counted in the forward and backward detectors, respectively, and α is an instrumental calibration factor. ZF-μSR study was carried out with detectors in a longitudinal configuration, where a correction coil is used to reduce any stray magnetic fields to below 1 μT. ZF-μSR measurements are crucial to understand the type of pairing symmetry in superconductors [26]. TF-μSR measurements were carried out in the vortex state in the presence of 10-, 20-, 30-, and 40-mT applied fields, which are above the lower critical field $\mu_0 H_{c1}(0)$ (= 0.7 mT) and below the upper critical field $\mu_0 H_{c2}(0)$ (= 0.6 T). The sample was mounted onto a high-purity (99.995%) silver sample holder using diluted GE varnish and then wrapped with thin silver foil. This was inserted in the sample chamber using a dilution refrigerator that can go down to 50 mK. We analyzed the μSR data using the WIMDA [28] software.

III. RESULTS AND DISCUSSION

A. Crystal structure and resistivity

The powder x-ray diffraction data revealed that ZrIrSi crystallizes in the orthorhombic structure (space group *Pnma*) as displayed in Fig. 1(a). The calculated lattice parameters are $a = 6.557(3)$ Å, $b = 3.942(6)$ Å, and $c = 7.413(4)$ Å, which are in agreement with a previous report [20]. The temperature (T) variation of the electrical resistivity $\rho(T)$ in the zero applied magnetic field is presented in Fig. 1(b). The electrical resistivity data reveals superconductivity at $T_C = 1.7$ K. Kase *et al.* [20] have estimated the Ginzburg Landau coherence length $\zeta = 23.1$ nm. It is interesting to note that the T dependence of the upper critical field shows a convex curvature [20], which might suggest the presence of SO coupling. Similar curvature is also found in $R_3T_4Sn_{13}$ (R = La or Sr; T = Rh or Ir), which is a SO-coupled superconductor [29].

B. TF-μSR analysis

To explore the pairing mechanism and gap structure of the superconducting state of ZrIrSi, TF-μSR measurements were performed down to 0.05 K. Figures 1(c)–1(f) present the TF-μSR asymmetry time spectra in the presence of 10 and 30 mT applied magnetic fields at temperatures above and below T_C. Below T_C the spectra depolarizes strongly because of the inhomogeneous field distribution in the vortex state. TF-μSR data were fit using two Gaussian oscillatory functions [30–32]:

$$G_{TF}(t) = \sum_{i=1}^{2} A_i \cos(\omega_i t + \phi) \exp\left(-\frac{\sigma_i^2 t^2}{2}\right), \qquad (1)$$

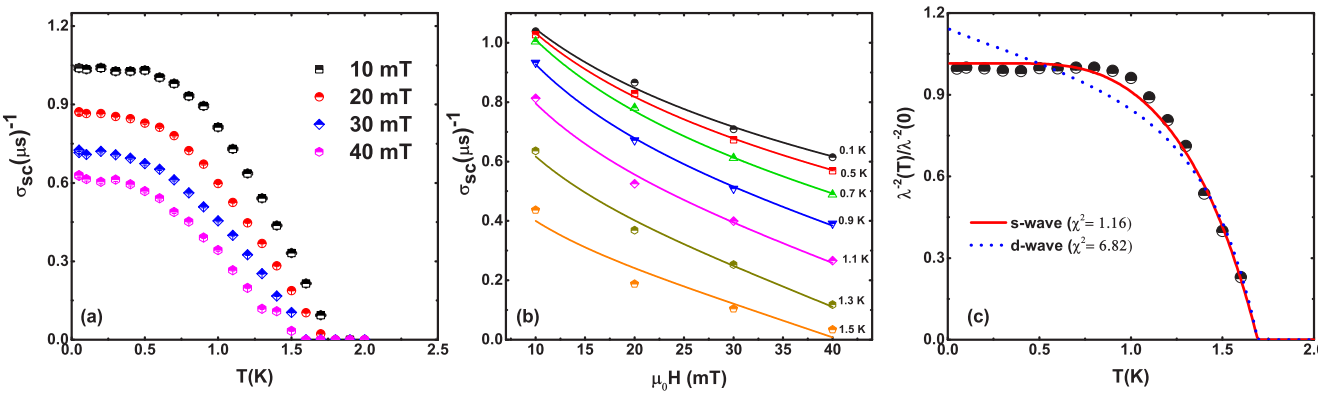

FIG. 2. (a) The superconducting depolarization rate $\sigma_{sc}(T)$ as a function of temperature in the presence of an applied field of $10 \leqslant \mu_0 H \leqslant 40$ mT. (b) The magnetic field dependence of the muon spin depolarization rate is shown for a range of different temperatures. The solid lines are the results of fitting the data using Brandt's equation as discussed in Eq. (2). (c) The inverse magnetic penetration depth squared as a function of temperature is shown here. The lines show the fits using s-wave (solid) and d-wave (dashed) gap functions.

where A_i, σ_i, ω_i, and ϕ is the initial asymmetry, the Gaussian relaxation rate, the muon spin precession frequency, and the initial phase of the offset, respectively. In this fit $\sigma_2 = 0$. This background term arises from those muons that missed the sample and were directly implanted into the silver sample holder and so do not depolarize as silver has a minimal nuclear moment. σ_1 can be expressed as $\sigma_1 = \sqrt{\sigma_{sc}^2 + \sigma_n^2}$, where σ_{sc} comes from the superconducting part and σ_n comes from nuclear magnetic dipolar moment which is fixed in the entire temperature range, as supported by the ZF-μSR data presented later.

The temperature variation of σ_{sc} is depicted in Fig. 2(a). As the H_{c2} value is low in this sample, σ_{sc} depends on the applied field as displayed in Fig. 2(b). Brandt [33,34] has reported that, for a superconductor with $H_{ext}/H_{c2} \leqslant 0.25$, σ_{sc} is associated with the magnetic penetration depth $[\lambda(T)]$ by the following equation:

$$\sigma_{sc}[\mu s^{-1}] = 4.83 \times 10^4 (1 - H_{ext}/H_{c2}) \times \{1 + 1.21[1 - \sqrt{(H_{ext}/H_{c2})}]^3\}\lambda^{-2}\ [\text{nm}]. \quad (2)$$

This equation is a good approximation for $\kappa \geqslant 5$, where $\kappa = \lambda/\xi$ (λ is the magnetic penetration depth and ξ is the superconducting coherence length), which is valid for our case as $\kappa = 40.5$ for ZrIrSi [20]. From this relation we have determined the temperature dependence of $\lambda(T)$ and $\mu_0 H_{c2}(T)$. Isothermal cuts perpendicular to the temperature axis of σ_{sc} data sets were used to determine the H dependence of the depolarization rate $\sigma_{sc}(H)$ as displayed in Fig. 2(b). We have estimated the magnetic penetration depths, $\lambda = 254.4(3)$ nm, using an s-wave model.

We have plotted the temperature variation of normalized $\lambda^{-2}(T)/\lambda^{-2}(0)$, which is directly proportional to the superfluid density. $\lambda^{-2}(T)/\lambda^{-2}(0)$ data were fitted using the following equation [35–39]:

$$\frac{\sigma_{sc}(T)}{\sigma_{sc}(0)} = \frac{\lambda^{-2}(T)}{\lambda^{-2}(0)} = 1 + \frac{1}{\pi}\int_0^{2\pi}\int_{\Delta(T)}^{\infty}\left(\frac{\delta f}{\delta E}\right)\frac{E dE d\phi}{\sqrt{E^2 - \Delta(T)^2}}. \quad (3)$$

Here f is the Fermi function which can be expressed as $f = [1 + \exp(-E/k_B T)]^{-1}$. $\Delta(T, 0) = \Delta_0 \delta(T/T_C) g(\phi)$; where $g(\phi)$ is the angular dependence of the gap function, ϕ is the azimuthal angle in the direction of Fermi surface. The temperature variation of the superconducting gap is approximated by the relation $\delta(T/T_C) = \tanh\{1.82[1.018(T_C/T - 1)]^{0.51}\}$. The spatial dependence $g(\phi)$ is substituted by (i) 1 for an s-wave gap and (ii) $|\cos(2\phi)|$ for a d-wave gap with line nodes.

Figure 2(c) presents the fits to the $\lambda^{-2}(T)/\lambda^{-2}(0)$ data of ZrIrSi using a single-gap s-wave model and a nodal d-wave model. It is clear that the data can be well described by the isotropic s-wave model with a gap value of 0.37(1) meV. This model gives a gap to the T_C ratio, $2\Delta(0)/k_B T_C = 5.10(2)$. The higher value of the gap compared to the BCS gap (3.53) indicates a strong coupling superconductivity in ZrIrSi. Similar high gap values were obtained for Ir-based superconductors, for example: IrGe $[2\Delta(0)/k_B T_C = 5.14]$ [15,22] and $CaIrSi_3$ $[2\Delta(0)/k_B T_C = 5.4]$ [40]. On the other hand, the d-wave model is clearly not suitable for this system as the χ^2 value increased significantly for this fit ($\chi^2 = 6.82$). As ZrIrSi is a type II superconductor, supposing that approximately all the normal state carriers (n_e) contribute to the superconductivity ($n_s \approx n_e$, where n_s is the superconducting carrier density), the effective-mass enhancement m^* values have been estimated to be $n_s = 6.9(1) \times 10^{26}$ carriers m^{-3} and $m^* = 1.474(3)\, m_e$, respectively, for ZrIrSi. Detailed calculations can be found in Refs. [41–43].

C. ZF-μSR analysis

In order to investigate the pairing mechanism in the superconducting ground state, we have performed a ZF-μSR study. The time evolution of asymmetry spectra is shown in Fig. 3 for $T = 0.05$ K $< T_C$ and $T = 2$ K $> T_C$. The spectra below and above T_C are found to be identical, ruling out the presence of any magnetic field. This reveals that TRS is preserved in the superconducting state of ZrIrSi. This ZF data were fit by a Lorentzian function:

$$G_{ZF}(t) = A_0(t)\exp(-\lambda t) + A_{bg}, \quad (4)$$

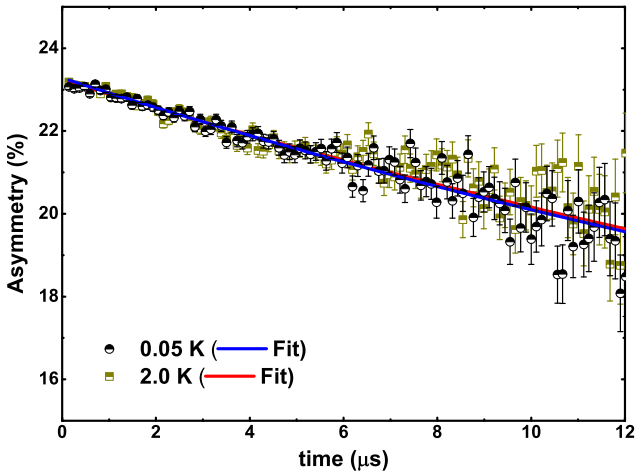

FIG. 3. ZF-μSR asymmetry time spectra for ZrIrSi at 0.05 K (black circles) and 2 K (dark yellow squares) are shown together. The lines are the least-squares fits to the data using Eq. (4).

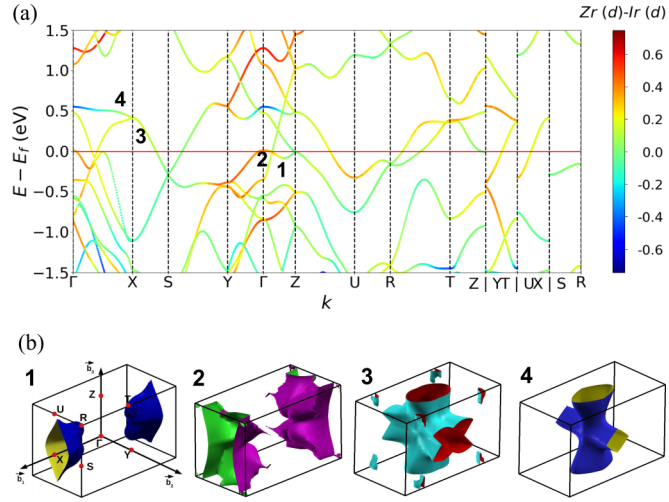

FIG. 4. (a) Computed DFT band structure is plotted along the standard high-symmetric directions for the orthorhombic crystal structure of ZrIrSi. The bands are colored with the difference in the d-orbital weight of the Zr and Ir atoms, where red color gives stronger Zr d-orbital weight while blue color dictates Ir d-orbital weight. Four bands which pass through the Fermi level are indicated by 1, 2, 3, 4 numbers. (b) Corresponding Fermi surfaces are plotted in the full three-dimensional Brillouin zone. We find that Fermi surface 1 and 2 form pockets around the X point, while Fermi surface 3 and 4 constitute pockets centering the Γ point. The colors on the Fermi surface only aid visualization.

where A_0 and A_{bg} are the sample and background asymmetry, respectively, which are nearly temperature independent. λ is the relaxation rate which comes from nuclear moments. The red and blue lines in Fig. 3 indicate the fits to the ZF-μSR data. The fitting parameters of the ZF-μSR asymmetry data are as follows: $\lambda = 0.030(9)\ \mu s^{-1}$ at 0.05 K and $\lambda = 0.026(3)\ \mu s^{-1}$ at 2 K. The change in the relaxation rate is within the error bar and indicates no clear evidence of TRS breaking in ZrIrSi.

D. Theoretical calculations

ZrIrSi unit-cell has an *mmm* point group symmetry and it belongs to the *Pnma*(*62*) space group (orthorhombic crystal structure). We have used the Vienna Ab-initio Simulation Package (VASP) for *ab initio* electronic structure calculation. The projector augmented wave (PAW) pseudopotentials are used to describe the core electrons, and for the exchange-correlation functional, the Perdew-Burke-Ernzerhof form is used. We have used a local density application (LDA) functional with a cutoff energy for the plane-wave basis set of 500 eV. The Monkhorst-Pack k-mesh is set to $14 \times 14 \times 14$ in the Brillouin zone for the self-consistent calculation. The optimized lattice parameters by energy minimization were found to be as follows: $a = 3.9643$ Å, $b = 6.5893$ Å, and $c = 7.4070$ Å, and $\alpha = \beta = \gamma = 90^\circ$. To deal with the strong correlation effect of the d electrons of the Ir atoms, we employed the LDA + U method with $U = 2.8$ eV. For the Fermi surface calculation, we used a larger k mesh of $31 \times 31 \times 31$.

In Fig. 4, we show the band structure and the Fermi surface plots. We find that there are four bands passing through the Fermi level, forming four Fermi surface pockets. Two Fermi pockets are centered around the Γ point, while the other two pockets are centered around the X point. Unlike the multigap superconductivity in MgB_2 [44] and Mo_8Ga_{41} [45] which are driven by the presence of multiple Fermi surfaces, we do not find any evidence of multigap superconductivity in ZrIrSi, which is in agreement with the TF-μSR results. This is presumably because of the absence of the E_{2g}-phonon mode which could enable interband scattering, while in the present case phonon modes cause intraband electron-phonon coupling. Moreover, we observe substantial three-dimensionality in all four Fermi surfaces. This substantially weakens the Fermi surface nesting strength. Thus the possibility of an interband nesting driven by unconventional $s^{\pm}$-pairing symmetry is suppressed as compared to a two-dimensional iron-pnictide family with similar Fermi surface topology (see, e.g., Ref. [46]).

Finally, we study the orbitals' contributions to the low-energy electronic states. We find that the low-energy bands are dominated by the 4d orbitals of the transition metal Zr, with substantially less weight from the 5d orbitals of the Ir atoms. Due to the presence of d orbitals in the low-energy states, it is natural to anticipate the involvement of strong correlation in these systems and hence strong coupling superconductivity which changes from the typical electron-phonon mechanism to a quasiparticle-phonon mechanism within the Eliashberg theory [47]. However, to our surprise, we find a substantially lower effective mass of $1.5m_e$ (where m_e is the bare electron's mass), which is in remarkable agreement with the results from the TF-μSR measurements. This is well captured within our LDA + U calculation without essentially including dynamical correlations. We repeated the calculations for the isostructural compounds TiIrSi and HfIrSi and found that the essential Fermi surface topology and three-dimensionality remain the same in all three materials (not shown). Therefore, we conclude that the superconductivity in ZrIrSi and its isostructural materials (such as TiIrSi and HfIrSi) can be well understood within the conventional BCS theory. Although our estimate of

the BCS ratio of 5.1 is slightly higher than the BCS estimate of 3.5, we believe this slight increment is caused by the spin-orbit coupling of the Ir atoms and by the Fermi surface anisotropy.

IV. CONCLUSIONS

In conclusion, we have performed ZF- and TF-μSR measurements in the mixed state of ZrIrSi. Using Brandt's equation we have determine the temperature dependence of the magnetic penetration depth. The superfluid density $n_s \propto 1/\lambda^2$ is well described by an isotropic *s*-wave model. The obtained gap value is $2\Delta(0)/k_B T_C = 5.10(2)$, which suggest ZrIrSi to be a strongly coupled BCS superconductor. *Ab initio* electronic structure calculation indicates BCS superconductivity, which supports our experimental results. The low-energy bands are dominated by the 4*d* orbitals of the transition metal Zr, with a substantially less weight from the 5*d* orbitals of the Ir atoms. ZF-μSR reveals there is no spontaneous magnetic field below T_C, which suggest the absence of TRS breaking. The present results pave the way to develop a realistic theoretical model to interpret the origin of superconductivity in ternary systems.

ACKNOWLEDGMENTS

K.P. acknowledges financial support from DST, India, under Inspire Fellowship No. IF170620. A.B. acknowledges DST, India, for Inspire Faculty Research Grant No. DST/INSPIRE/04/2015/000169 and UK-India Newton funding for funding support. D.T.A. thanks the Royal Society of London for the UK-China Newton funding and the JSPS for the invitation fellowship. T.D. acknowledges the financial support from the Science and Engineering Research Board (SERB), Department of Science & Technology (DST), Government of India, for the Start-Up Research Grant (Young Scientist).

[1] H. Barz, H. C. Ku, G. P. Meisner, Z. Fisk, and B. T. Matthias, Proc. Natl. Acad. Sci. USA **77**, 3132 (1980).
[2] R. Müller, R. N. Shelton, J. W. Richardson, and R. A. Jacobson, J. Less-Common Met. **42**, 177 (1983).
[3] D. K. Seo, J. Ren, M. H. Whangbo, and E. Canadell, Inorg. Chem. **36**, 6058 (1997).
[4] W. Y. Ching, Y. N. Xu, L. Ouyang, and W. Wong-Ng, J. Appl. Phys. **93**, 8209 (2003).
[5] H. Keiber, H. Wühl, G. P. Meisner, and G. R. Stewart, J. Low Temp. Phys. **55**, 11 (1984).
[6] I. Shirotani, M. Takaya, I. Kaneko, C. Sekine, and T. Yagi, Physica C (Amsterdam, Neth.) **357–360**, 329 (2001).
[7] I. Shirotani, Y. Konno, Y. Okada, C. Sekine, S. Tado, and T. Yagi, Solid State Commun. **108**, 967 (1998).
[8] I. Shirotani, M. Takeya, I. Kaneko, C. Sekine, and T. Yagi, Solid State Commun. **116**, 683 (2000).
[9] I. Shirotani, K. Tachi, Y. Konno, S. Todo, and T. Yagi, Phil. Mag. Part B **79**, 767 (1999).
[10] I. Shirotani, K. Tachi, K. Takeda, S. Todo, T. Yagi, and K. Kanoda, Phys. Rev. B **52**, 6197 (1995).
[11] I. Shirotani, N. Ichihashi, K. Nozawa, M. Kinoshita, T. Yagi, K. Suzuki, and T. Enoki, Jpn. J. Appl. Phys. **32**, 695 (1993).
[12] G. P. Meisner, H. C. Ku, and H. Barz, Mater. Res. Bull. **18**, 983 (1983).
[13] S. Pyon, K. Kudo, J. Matsumura, H. Ishii, G. Matsuo, M. Nohara, H. Hojo, K. Oka, M. Azuma, O. Garlea, K. Kodama, and S. Shamoto, J. Phys. Soc. Jpn. **83**, 093706 (2014).
[14] H. Y. Lu, N. N. Wang, L. Geng, S. Chen, Y. Yang, W. J. Lu, W. S. Wang, and J. Sun, Europhys. Lett. **110**, 17003 (2015).
[15] B. T. Matthias, T. H. Gkballk, and V. B. Compton, Rev. Mod. Phys. **35**, 1 (1963).
[16] N. Haldolaarachchige1, L. Schoop, M. A. Khan, W. Huang, H. Ji, K. Hettiarachchilage, and D. P. Young, J. Phys.: Condens. Matter **29**, 475602 (2017).
[17] Y. J. Sato, A. Nakamura, Y. Shimizu, A. Maurya, Y. Homma, D. Li, F. Honda, and D. Aoki, J. Phys. Soc. Jpn. **87**, 053704 (2018).
[18] A. Bhattacharyya, D. T. Adroja, P. K. Biswas, Y. J. Sato, M. R. Lees, D. Aoki, and A. D. Hillier, arXiv:1901.04796.
[19] N. Haldolaarachchige, Q. Gibson, L. M. Schoop, H. Luo, and R. J. Cava, J. Phys. Condens. Matter **27**, 185701 (2015).
[20] N. Kase, H. Suzuki, T. Nakano, and N. Takeda, Supercond. Sci. Technol. **29**, 035011 (2016).
[21] U. Pfannenschmidt, U. C. Rodewald, and R. P. Ottgen, Z. Naturforsch., B: J. Chem. Sci. **66**, 205 (2011).
[22] A. S. Cuamba, H.-Y. Lu, and C. S. Ting, Phys. Rev. B **94**, 094513 (2016).
[23] A. Bhattacharyya, D. T. Adroja, J. Quintanilla, A. D. Hillier, N. Kase, A. M. Strydom, and J. Akimitsu, Phys. Rev. B **91**, 060503(R) (2015).
[24] A. Bhattacharyya, D. T. Adroja, N. Kase, A. Hillier, J. Akimitsu, and A. M. Strydom, Sci. Rep. **5**, 12926 (2015).
[25] A. Bhattacharyya, D. T. Adroja, N. Kase, A. D. Hillier, A. M. Strydom, and J. Akimitsu, Phys. Rev. B **98**, 024511 (2018).
[26] J. E. Sonier, J. H. Brewer, and R. F. Kiefl, Rev. Mod. Phys. **72**, 769 (2000).
[27] S. L. Lee, S. H. Kilcoyne, and R. Cywinski, *Muon Science: Muons in Physics, Chemistry, and Materials* (SUSSP and IOP, Bristol, England, 1999).
[28] F. L. Pratt, Physica B (Amsterdam, Neth.) **289–290**, 710 (2000).
[29] N. Kase, H. Hayamizu, and J. Akimitsu, Phys. Rev. B **83**, 184509 (2011).
[30] A. Bhattacharyya, D. T. Adroja, M. Smidman, and V. K. Anand, Sci. China: Phys., Mech. Astron. **61**, 127402 (2018).
[31] D. Adroja, A. Bhattacharyya, P. K. Biswas, M. Smidmann, A. D. Hillier, H. Mao, H. Luo, G. H. Cao, Z. Wang, and C. Wang, Phys. Rev. B **96**, 144502 (2017).
[32] A. Bhattacharyya, D. T. Adroja, K. Panda, S. Saha, T. Das, A. J. S. Machado, O. V. Cigarroa, T. W. Grant, Z. Fisk, A. D. Hillier, and P. Manfrinetti, Phys. Rev. Lett. **122**, 147001 (2019).
[33] E. H. Brandt, J. Low Temp. Phys. **73**, 355 (1988).
[34] E. H. Brandt, Phys. Rev. B **68**, 054506 (2003).

[35] R. Prozorov and R. W. Giannetta, Supercond. Sci. Technol. **19**, R41 (2006).
[36] D. T. Adroja, A. Bhattacharyya, M. Telling, Y. Feng, M. Smidman, B. Pan, J. Zhao, A. D. Hillier, F. L. Pratt, and A. M. Strydom, Phys. Rev. B **92**, 134505 (2015).
[37] D. T. Adroja, A. Bhattacharyya, M. Smidman, A. D. Hillier, Y. Feng, B. Pan, J. Zhao, M. R. Lees, A. M. Strydom, and P. K. Biswas, J. Phys. Soc. Jpn. **86**, 03470 (2017).
[38] D. Das, R. Gupta, A. Bhattacharyya, P. K. Biswas, D. T. Adroja, and Z. Hossain, Phys. Rev. B **97**, 184509 (2018).
[39] A. Bhattacharyya, D. T. Adroja, A. D. Hillier, R. Jha, V. P. S. Awana, and A. M. Strydom, J. Phys: Condens. Matter **29**, 265602 (2017).
[40] R. P. Singh, A. D. Hillier, D. Chowdhury, J. A. T. Barker, D. McK. Paul, M. R. Lees, and G. Balakrishnan, Phys. Rev. B **90**, 104504 (2014).
[41] A. D. Hillier and R. Cywinski, Appl. Magn. Reson. **13**, 95 (1997).
[42] D. T. Adroja, A. D. Hillier, J.-G. Park, E. A. Goremychkin, K. A. McEwen, N. Takeda, R. Osborn, B. D. Rainford, and R. M. Ibberson, Phys. Rev. B **72**, 184503 (2005).
[43] V. K. Anand, D. Britz, A. Bhattacharyya, D. T. Adroja, A. D. Hillier, A. M. Strydom, W. Kockelmann, B. D. Rainford, and K. A. McEwen, Phys. Rev. B **90**, 014513 (2014).
[44] Amy Y. Liu, I. I. Mazin, and J. Kortus, Phys. Rev. Lett. **87**, 087005 (2001).
[45] A. Sirohi, S. Saha, P. Neha, S. Das, S. Patnaik, T. Das, and G. Sheet, Phys. Rev. B **99**, 054503 (2019).
[46] P. J. Hirschfeld, M. M. Korshunov, and I. I. Mazin, Rep. Prog. Phys. **74**, 124508 (2011); T. Das, EPJ Web Conf. **23**, 00014 (2012).
[47] T. Das and K. Dolui, Phys. Rev. B **91**, 094510 (2015).